An elementary model of nonexponential decay. II. Applications to measurements in superconductors and in a spin glass

1994 J. Phys.: Condens. Matter 6 2893

(http://iopscience.iop.org/0953-8984/6/15/012)

J. Phys.: Condens. Matter 6 (1994) 2893–2910. Printed in the UK

An elementary model of non-exponential decay: II. Applications to measurements in superconductors and in a spin glass

P Erhart, B Senning and F Waldner
Physics Institute, University of Zürich, CH-8057 Zürich, Switzerland

Received 7 July 1993, in final form 19 January 1994

Abstract. The 'elementary decay model' (EDM), which allows an interpretation of most non-exponential decay functions, is applied to representative published decay curves measured in superconductors and in a metallic spin glass. Features attributed previously to different regimes connected by crossover regions can be interpreted by monotonically changing parameters.

For high-T_c superconductors I–V curves are also analysed with the adequately transformed EDM. In addition, the excess conductivity in the paraconductive region above T_c is well modelled by an Arrhenius excitation, which also extends below T_c in multilayers of YBCO. Measurements previously interpreted by $U_{\text{eff}} \propto J^{-\mu}$ can also be interpreted by the EDM, which is close to $U_{\text{eff}} \propto -\ln J$ evaluated by Blatter and co-workers. The rapid drop in resistivity close to a transition into a vortex–glass state measured in the pV range by Gammel and co-workers in YBCO could also be fitted by the EDM.

Further, the 'ageing' or 'memory' effect in a metallic spin glass is well interpreted by the EDM. In particular, the 'memory' effect is shown to be a consequence of plotting non-exponential decay data against the logarithm of a retarded time and is therefore not a unique indication for a spin glass.

1. Introduction

In the previous paper [1], an elementary decay model (EDM) was introduced that interpreted quantitatively most non-exponential normalized decay forms $x(t) = X(t)/X_0$ as observed in, and proposed for, disordered structures such as spin glasses and granular superconductors.

The EDM can be considered as generated by an initial distribution $f_0(E')$ of occupied activation energies $E' = E/T$ with their occupation decaying independently in time t by thermal activation with a rate $r_0 \exp(-E')$, and with $1/b = \bar{E}' = \bar{E}/T$ denoting the average initial energy $\bar{E}$ normalized by the temperature T. The ratio $\bar{E}/T = 1/b(T)$ determines the shape, with an exponential form for $b \to \infty$, a form close to a power law for intermediate values of $b(T)$, and a nearly logarithmic decay for $b(T) \ll 1$. Intermediate values of $b(T)$ also describe the 'crossover' regions quantitatively.

On the other hand, the EDM could be regarded as generated by an effective activation energy $U_{\text{eff}}(x)$ which increases in time as a function of the decaying normalized observable x.

The resulting functions of the EDM were compared in [1] with existing predictions of microscopic models for decay in spin glasses and superconductors.

The first decay data in a high-T_c superconductor published by Müller and co-workers [2], who were also the first to propose a spin-glass-type behaviour, have already been fitted [3].

The present paper applies the EDM to selected experimental data in superconductors and in a metallic spin glass.

0953-8984/94/152893+18$19.50

2. The 'elementary decay model' (EDM)

Since the 'elementary decay model' (EDM) has already been introduced [1], only a brief description will be given here.

The motivation was to search for an elementary common physical mechanism for the non-exponential decay observed in a large number of disparate phenomena. Probably the most elementary assumption is an initial Poissonian $f_0(E') = (1/\bar{E}')\exp(-E'/\bar{E}')$ distribution of activation energies $E' = E/T$, with normalized average energy $\bar{E}' = \bar{E}/T$ and with each fraction decaying independently according to an Arrhenius rate $r(E') = r_0\exp(-E')$. The resulting normalized form $g(b, \tau) = X(t)/X_0$ of the EDM for the above elementary initial condition could be evaluated in closed form

$$g(b, \tau) = b\tau^{-b}\gamma(b, \tau) = b\tau^{-b}\int_0^\tau s^{b-1}e^{-s}\,ds \tag{1}$$

with the normalized time $\tau = r_0 t$ and with the incomplete gamma function $\gamma(b, \tau)$ as an important correction to the term τ^{-b} describing a power law.

In an alternative interpretation, this decay form $g(b, \tau)$ could also be considered as generated by a b-dependent form of an effective barrier energy $U_{\text{eff}}(g)$ increasing as a function of the decaying normalized observable g.

A very simple method to vary the shape of a non-exponential function consists in shifting the starting time from $t = 0$ to a new starting time $t^* = 0$ by a fictive initial delay t_{in} where $t = t^* + t_{\text{in}}$, with the resulting function renormalized to one for $t^* = 0$. This method has been used to generalize the EDM to describe variations of the short time behaviour by introducing a second parameter $\tau_{\text{in}} = r_0 t_{\text{in}}$ yielding a normalized two-parameter decay:

$$g^{(2)}(b, \tau_{\text{in}}; \tau^*) = \frac{g(b, \tau = \tau^* + \tau_{\text{in}})}{g(b, \tau_{\text{in}})|_{\tau^*=0}}. \tag{2}$$

A variation of the long time behaviour will be treated in section 3.1.4, where the extended exponential $\exp[-(t/t_0)^\beta]$ (the Kohlrausch function) is approximated.

3. Application of the EDM to experimental data

3.1. Fitting decay measurements in superconductors

3.1.1. Effective activation energy in high-T_c superconductors. Maley and co-workers [4] obtained the dependence of the effective activation energy U_{eff} as a function of the magnetization from magnetic relaxation studies in YBCO. Data points obtained similarly by van der Beek and co-workers [5] in a $Bi_2Sr_2CaCu_2O_{8+\delta}$ single crystal are reproduced in figure 1 together with the fit with the corresponding curve for $U_{\text{eff}}^{/(r)}(x)$ obtained from the EDM with $b = 0.07$. Note that the log–log plot yields a curved function. The interpretation [6, 7] by a power law $U_{\text{eff}} \propto (\check{J})^{-\mu}$, where $\check{J} = J/J_c$, is shown by broken curves for the exponents $\mu = 9/8$ predicted [8] for the thermal activation of small flux bundles in a weakly pinned 3D vortex lattice, and $\mu = 1/2$ for the activation of larger bundles [9].

The experimental data indicate a rather continuous 'crossover' of the exponent μ, similar to the result found in a Monte Carlo simulation [10] of the Sherrington–Kirkpatrick model (see figure 8 of the previous paper).

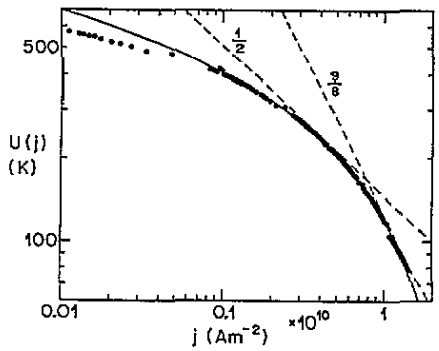

Figure 1. Points (from [5]): dependence on current density of the extracted effective barrier $U(j)$ on a log–log plot. Curves: fits of $U_{\rm eff}^{\prime r}(j)$ of the EDM with $b = 0.08$.

3.1.2. Combining decay and I–V curves of a high-T_c superconductor. Sandvold and Rossel [11] combined I–V characteristics and magnetic relaxation in YBCO films measured at 70 K ($T_c = 88.5$ K). The analysis of the magnetic relaxation $M(t)$ in a ring revealed an electric field $E(J)$ as a function of the current density J, with E ten orders of magnitude lower than for the I–V measurements. Both types of measurements were performed at 1 and 3 kG. The four resulting sets of measurements are well described by the same form $\ln(E) = A - B/(DJ)^C$ as predicted by the collective pinning theory and in the vortex–glass model which assume $U_{\rm eff} \propto J^{-1/\alpha}$ in the expression for the electric field $E \propto \exp(-U_{\rm eff}/T)$ in the regime of collective creep occurring below the irreversibility line. The authors used the same exponent $C = 1/\alpha$ for all four sets, yielding $\alpha = 2.9 \pm 0.4$. However, the fitting parameters A and B were different for the two magnetic field settings, and three different values for D were used. Hence the four sets were fitted with the eight parameters $A_1, A_3, B_1, B_3, C, D_{I-V,1}, D_{I-V,3}, D_M$ and thus with two adjustable parameters for each set.

In the framework of the EDM each set of measurements can independently be fitted with two adjustable parameters $\mathcal{A}_i$ and $\mathcal{B}_i$. Using the approximations $E(J) = \mathcal{A}_i J^{\mathcal{B}_i+1}$ for the I–V data and $M(t) = \mathcal{A}_i t^{-\mathcal{B}_i}$ for the magnetic relaxation, the resulting values for $\mathcal{B}_i = \tilde{E}_i/T = 1/b$ are around 28, 22 for the I–V data and 34, 29 for the $M(t)$ data for 1 kG and 3 kG, respectively, thus decreasing for increasing magnetic and electric fields, with the same ratio as the authors' values $\hat{U}_0/kT \approx 70, 55$ for the I–V data.

In contrast to Sandvold and Rossel, the interpretation by the EDM yields the above four independent values for the average energies $\mathcal{B}_i = \tilde{E}_i/T$, without a common exponent, as in the glass model with the effective energy $U_{\rm eff}/T \propto J^{-C}$.

However, an arbitrary common exponent C could be constructed for $\mathcal{B}_i = \mathcal{F}(\mathcal{D}_i\mathcal{J}_i)^{-C}$. This is possible by setting $\mathcal{D}_1 = 1$, which defines the common prefactor $\mathcal{F}$. Then the remaining three scaling factors $\mathcal{D}_i$ are determined. Such a calculation could obviously be performed for any set of four positive pairs $(\mathcal{B}_i, \mathcal{J}_i)$ and chosen non-zero value for an exponent C.

Therefore, the uniqueness of the interpretation by $U \propto J^{-C}$ with a common exponent C might be reconsidered if the fits of different sets imply that the measured current densities have to be scaled by different adjustable factors D_i. The difference between the two interpretations would then be reduced to the question: is the small negative curvature in the log–log scale inside each data set relevant? In the I–V data the curvature occurs for the data below $E = 10^{-5}\,\mathrm{V\,cm^{-1}}$ where the scatter of the data is increased, and for the $M(t)$

data in the region close to the well pronounced systematic deviation of the magnetometer.

3.1.3. Decay in an extreme type-II superconductor. The decay functions observed by Svedlindh and co-workers [12] in the extreme type-II superconductor $PbMo_6S_8$ show a strong dependence on the applied magnetic field for small fields, but are nearly independent for high fields. As an example, see figure 5(*b*) of [12]; the authors fitted at a high field the decay of the thermoremanent magnetization $M(t) = A[\ln t/t_0]^{-\alpha}$ yielding $\alpha = 1.25 \pm 0.1$ and $\log_{10}(t_0) = -9 \pm 1$ at 13.5 K. Furthermore, the authors tried to fit a power law $t^{-\beta}$, but they could not find a good description of the observed data.

These data measured at 13.5 K are used for a comparison of different quantitative descriptions. The resulting relative deviations are plotted in figure 2.

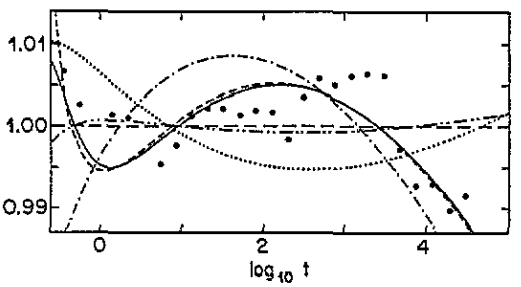

Figure 2. The decay of the thermoremanent magnetization $M(t)$ in the extreme type-II superconductor $PbMo_6S_8$ observed at high fields at 13.5 K by Svedlindh and co-workers [12] is fitted with the following functions. For selected measured data [12] the ratio $M_{measured}/M_{fit}$ (points) are displayed after fitting to (α.3). The other fits are represented by curves. (i) (α) $A[\ln t/t_0]^{-\alpha}$. (α.1) ····· fit with the values of [12] kept within their errors. (α.2) — · · — fit with α, t_0 and A as free parameters, yielding $\alpha = 1.55 \pm 0.03$, $\log_{10}(t_0) = -11.7 \pm 0.3$, and $A = 1400 \pm 200$. (α.3) — — — fit as (α.2), but with t replaced by $t + t_{corr}$, thus with t_{corr} as an additional free parameter, yielding $\alpha = 1.73 \pm 0.03$, $\log_{10}(t_0) = -13.3 \pm 0.3$, $A = 3100 \pm 400$, and $t_{corr} = (-0.03 \pm 0.05)$ s. (ii) (β) power law $B[r_0(t + t_{corr})]^{-\beta}$. ($\beta$.1) — · — fit with t_{corr} set to zero resulted in a large least-square deviation, see below. (β.2) - - - - fit with t_{corr} as an additional free parameter, yielding $\beta = 0.048 \pm 0.001$, $r_0 = (3.4 \pm 26)\text{s}^{-1}$, $B = 9 \pm 3$, and a correction of $t_{corr} = (-0.17 \pm 0.03)$ s. (g) —— $X_0 g^{(2)}[b, r_0(t + t_{corr})]$ of the EDM, with b, r_0, X_0 and t_{corr} as free parameters, yielding $b = 0.0482 \pm 0.0002$, $r_0 = (7.7193 \pm 0.0004)\,\text{s}^{-1}$, $X_0 = 9.33 \pm 0.02$ and $t_{corr} = (-0.2016 \pm 0.000\,03)$ s. This correction time could also be considered as a fictive time delay t_{ln} of the two-parameter function $g^{(2)}$ describing a different initial condition. The least square deviations χ^2 of the above examples relative to $\chi^2(g)$ are (α) 5.2, 2.0, 1.7; (β) 5.9, 1.1; and (g) 1.

Keeping in mind that fits are sensitive to the definition of the initial time $t = 0$ to be determined by the time when the field is switched off, the possibility of a small systematic deviation t_{corr} has been introduced by using $t + t_{corr}$ replacing their t.

The functions tested are (α) $A[\ln t/t_0]^{-\alpha}$, (β) power law $B[r_0(t + t_{corr})]^{-\beta}$, and ($g$) $X_0 g^{(2)}[b, r_0(t + t_{corr})]$ of the EDM.

As demonstrated by the deviations in figure 2, a power law can only be excluded if the actual time of the drop of the magnetic field is determined with high precision, i.e. when a value of t_{corr} around 0.2 s is improbable. Furthermore, for a clear discrimination between (α) and (g) the scatter of the data is too large.

Note that only the EDM allows a determination of the initial value X_0.

Moreover, their zero field cooled (ZFC) magnetizations M_{ZFC} measured at low magnetic fields are very peculiar. These data [12] exhibit an extremum in the derivative $dM/d(\ln t)$

with respect to the *logarithm* of the observation time t, see points in figure 3. The time when the extremum occurs increases for decreasing field. The authors [12] relate this extremum to a physical fact, namely 'to the time when full flux penetration in the sample is achieved'. Certainly, such an extremum might signal a special feature of the decay process. However, suppose a decay function $X(t)$ starts at a finite initial value X_0 with a finite derivative $-\mathrm{d}X/\mathrm{d}t$ with respect to time t and with $-\mathrm{d}X/\mathrm{d}t$ decreasing to zero for $t \to \infty$. This function will exhibit an extremum in their derivative $-\mathrm{d}X/\mathrm{d}(\ln t)$ at a time t_{extr} governed by the shape of $X(t)$, with $\tau_{\mathrm{extr}} = 1$ for $X(\tau) \propto \exp(-\tau)$ as an example, without the need for a change of the type of the decay at t_{extr}. This is demonstrated by fitting the observed decay with the double-parameter function $g^{(2)}(b, E'_{0-\mathrm{peak}}, \tau)$ of equation (6) of [1] of the EDM, see curves in figure 3. The resulting initial distributions $X_0 f_0(E')$ are displayed in the inset in figure 3. Note that the second describing parameter $E'_{0-\mathrm{peak}}$ is nearly independent of the applied field.

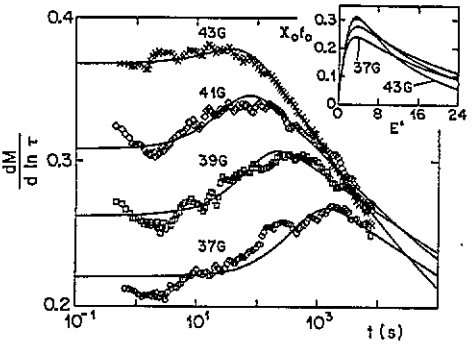

Figure 3. Derivative $\mathrm{d}M/\mathrm{d}(\ln t)$ of the zero field cooled magnetization M with respect to the logarithm of time t in the extreme type-II superconductor $PbMo_6S_8$ at small magnetic fields of 37, 39, 41 and 43 G, from Svedlindh and co-workers [12]. Curves: fits of the derivative $X_0 \mathrm{d}g^{(2)}(b, E'_{0-\mathrm{peak}}, \tau)/\mathrm{d}(\ln \tau)$ of the EDM with $\tau = r_0 t$ and the corresponding fit values $X_0 = 5.9, 7.2, 6.4, 5.3$; $b = 0.05, 0.05, 0.06, 0.09$; $E'_{0-\mathrm{peak}} = 3.34, 3.50, 3.44, 3.36$; $r_0 = 0.002, 0.013, 0.034, 0.040\ \mathrm{s}^{-1}$; respectively. Inset: initial distribution functions $X_0 f_0(E')$ against reduced energy $E' = E/T$ of the EDM.

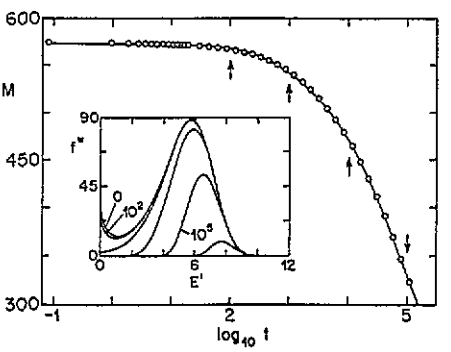

Figure 4. Points: relaxation of the remanent magnetization measured in the heavy fermion superconductor UPt_3 by Pollini and co-workers [13] at 209 mK. Curve: calculated decay using the heuristic form $f^{\mathrm{W}}(E', t) \propto (E'+1)^{(a-1)} \exp(-bE'^a) \exp[-(r_0 t + c)\exp(-E')]$ yielding $b = 0.0001$, $a = 4.8$, $r_0 = 0.0026$, $c = -5.5$. Inset: distributions $f^{\mathrm{W}}(E', t)$ for the times t=0, [10^2, 10^3, 10^4, 10^5, marked by arrows], 10^6. Except for the very short times, the decay is also well fitted by the Kohlrausch function $\exp[-(t/t_0)^\beta]$ with $\beta = 0.55$, $t_0 = 347$ s.

3.1.4. Decay in a heavy fermion superconductor. Another important example concerns the decay in the heavy fermion superconductor UPt_3 as reported by Pollini and co-workers [13], see points in figure 4. A stretched exponential $\exp[-(r_0 t)^\beta]$, the heuristic function of Kohlrausch, is an excellent description of the measured data, although there is at present no microscopic model that predicts the corresponding generating effective activation energy $U_{\mathrm{eff}}^{\prime(r)}(x) \propto (1-\beta^{-1}) \ln[-\ln x]$.

A description with a generating initial distribution according to (2)–(4) is not easy to find. The point is that, for a Kohlrausch behaviour, a Gaussian rather than a Poissonian distribution is adequate. Indeed, a heuristic modified Weibull initial distribution $f_0^{\mathrm{W}}(E')$

$$f_0^{\mathrm{W}}(E') \propto (E'+1)^{(a-1)} \frac{\exp(-bE'^a)}{\exp[\epsilon \exp(-E')]} \tag{3}$$

turned out to describe well the observed behaviour (see the full curve in figure 4, evaluated by numerical integration of equations (2) and (3) of [1]). The inset displays the distribution $f^{W}(E', t)$ for increasing times. Note that this asymmetric distribution goes through a symmetric distribution around $t = 10^5$, which is close to a *Gaussian* distribution.

3.2. The temperature-dependent decay in high-T_c superconductors

3.2.1. Adopting a temperature dependence for $\bar{E}$ of the EDM. Since the temperature dependence of the mean energy $\bar{E}$ of $b = T/\bar{E}$ is not part of this model and needs an understanding of the detailed physics involved, the form

$$\frac{1}{b} = \frac{\bar{E}}{T} = \frac{(1+\Theta^2)^{n/2}}{b_0\Theta(1-\Theta^2)^{n/2-2}} \tag{4}$$

of Hagen and Griessen [14] will be used with a variation of the heuristic parameter n.

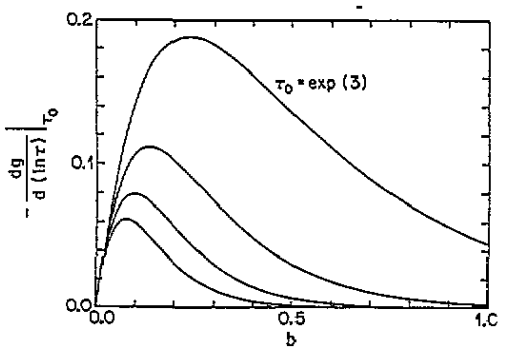

Figure 5. Derivative $-dg(b, \tau)/d(\ln\tau)|_{\tau_0}$ at four different fixed times τ_0 against decay parameter b with $\ln\tau_0 = 3$ (highest curve), 6, 9, 12 (lowest curve).

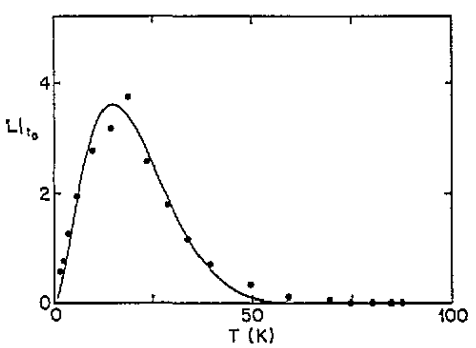

Figure 6. Points: experimental values of the derivative $L|_{t_0} = -dM/d(\ln t)|_{t_0}$ at a fixed time t_0 against temperature T from Hagen and Griessen [14]. Curve: corresponding $dX_0 g(b, \tau)/d(\ln\tau)|_{\tau_0}$ of the EDM assuming $b \propto \Theta(1-\Theta^4)^{-1}$, $X_0 \propto 1-\Theta$, $\ln\tau_0 = 9$, $T_c = 90$ K.

3.2.2. The logarithmic rate $-dX/d(lnt)|_{t_0}$ at fixed time t_0. For some experimental decay curves $X(t)$ measured at different temperatures T, the values of the derivative $L|_{t_0} = -dX/d(\ln t)|_{t_0}$ at a fixed time t_0 were plotted against T [14, 15].

In this context it is instructive to evaluate the corresponding EDM values $L_{EDM}|_{\tau_0} = -dg(b, \tau)/(d(\ln\tau)|_{\tau_0}$ at a fixed time τ_0 as a function of the parameter value $b = T/\bar{E}$. First, disregarding the present temperature dependence of $\bar{E}$, the corresponding values evaluated with the EDM are displayed as a function of a linearly increasing b in figure 5 for different

fixed times τ_0. Note that the function $L_{\mathrm{EDM}}|_{\tau_0}(b)$ has a maximum, although for increasing b the decay $g(\tau)$ is monotonically faster (see figure 1 of [1]). Further, the maximum of $L_{\mathrm{EDM}}|_{\tau_0}(b)$ in figure 5 depends on the value of the fixed time τ_0.

In order to compare with data measured by Hagen and Griessen [14] (shown in figure 6 as points), the approximate temperature dependence $\bar{E}/T \propto (1-\Theta^4)/\Theta$, with $\Theta = T/T_c$ proposed in [16], has been used for the average activation energy $\bar{E}$ in $b = T/\bar{E}$, i.e. equation (4) with $n = 2$.

Furthermore, using a simplified function for $X_0 \propto 1 - \Theta$, the curve in figure 6 approximates well the measured $L|_{t_0} = -\mathrm{d}M/\mathrm{d}(\ln t)|_{t_0}$. No physically relevant parameter peaks within the framework of the EDM; rather the peak is an artefact of plotting the derivative with respect to $\ln t$ of a non-logarithmic decay function at a fixed time t_0.

3.2.3. Temperature dependence of normalized $S|_{t_0} = -dlnX/d(lnt)|_{t_0}$. Malozemoff and Fisher [17] compared various measurements in YBaCuO by plotting the values $S|_{t_0} = -\mathrm{d}\ln M(t)/\mathrm{d}(\ln t)|_{t_0}$ at a fixed time t_0 as a function of temperature T. Later, Griessen and co-workers [18] collected additional experimental data which show that there is a large diversity of curves $S(T)$. However, it is remarkable that for intermediate temperatures most of the data are within the range $0.01 < S < 0.04$, that there is a clear tendency to decrease below 10 K, and that for the majority there is a plateau or a reduced slope of $S(T)$; the data of their figure 1 are reproduced in our figure 7. The temperature dependence (4) of Hagen and Griessen [14] has been used to display $S_{\mathrm{EDM}}(T)$ for various values of n in figure 7 (full curves).

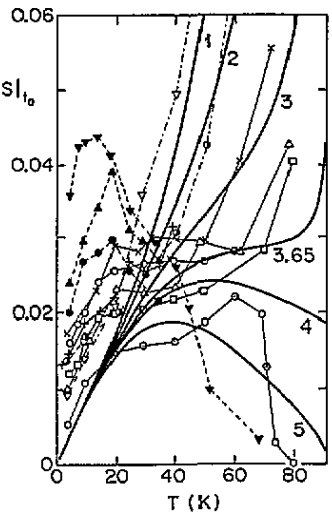

Figure 7. Points (from Griessen and co-workers [18]): normalized relaxation rate $S(T)|_{\tau_0} = -\mathrm{d}\ln M(t)/\mathrm{d}(\ln t)|_{t_0}$ for various $YBa_2Cu_3O_7$ samples. Curves: EDM using (4) for $b = b_0\Theta/[(1-\Theta^2)^{2-n/2}(1+\Theta^2)^{n/2}]$ with $b_0 = 0.075$, $n = 1$, ,2, 3.65, 4, 5 and $\tau_0 = 8$.

The function $S_{\mathrm{EDM}}(T)$ of the EDM corresponding to $S(T)$ is related to $-\mathrm{d}g/\mathrm{d}\tau$ of (9) by

$$S_{\mathrm{EDM}}|_{\tau_0} = -\frac{\tau_0}{g(b,\tau_0)}\left.\frac{\mathrm{d}g}{\mathrm{d}\tau}\right|_{\tau_0} = b\left(1 - \frac{\exp(-\tau_0)}{g(b,\tau_0)}\right). \tag{5}$$

Note that a power law $x(\tau) \propto \tau^{-b}$, which corresponds to an effective activation energy $U'_{\mathrm{eff}} \propto \ln(\check{J}^{-1})$, would result in $S(T) = b(T)$. Deviations are a consequence of the deviation of $g(b,\tau)$ from a power law, which is expressed by the incomplete gamma function $\gamma(b,\tau)$.

3.2.4. The initial distribution by Hagen and Griessen. It seems worthwhile to compare the distribution function $u(b, E'')$ of equation (8) of [1] (shown in figure 5 of [1]), with distribution functions $m(E^*)$ of Hagen and Griessen [14] (see their figure 3), evaluated from measurements made for $\tau = r_0 t \gg 1$ and interpreted with an extended Anderson-type creep theory. The authors incorporated both an effective pinning energy and a distribution of initial energies E^*. Figure 8 displays their distribution function (full curve), their log-normal distribution (broken curve). Thus the interpretation by the EDM suggests an explanation of the distribution found by inversion [14] as an aged elementary stochastic distribution, suggested also for the distributions evaluated by Theuss [19] (see section 1.3 of [1]).

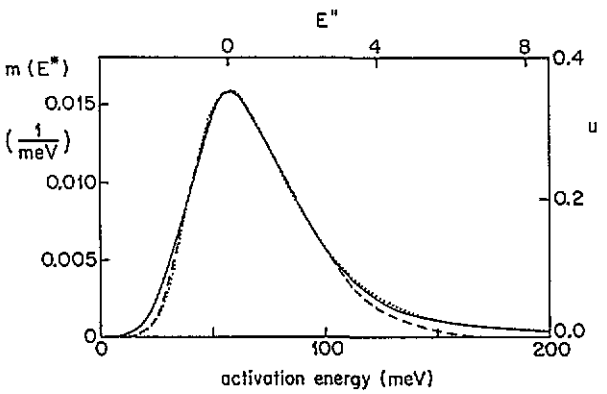

Figure 8. Full curve: initial distribution function $m(E^*)$ of activation energies E^* of Hagen and co-workers [14] as obtained from inverting experimental decay data. Broken curve: fit with a log-normal distribution. Pointed curve: corresponding distribution function $u(E' - E'_{peak})$ of the EDM, see equation (8) of [1], for $b = 0.62$.

3.3. Resistivity of high-T_c superconductors

3.3.1. The connection of decay and resistivity. As discussed in section 3.1 of [1], decay functions $x(t)$ are connected to the resistivity $\rho(x)$ by equation (11) of [1]

$$-\frac{dx}{d\tau} = x\check{r}_{eff}(x) \propto E(\check{J}) = \check{J}\rho(\check{J}) \tag{6}$$

with measurements of I–V current–voltage characteristics which yield the electric field $E(\check{J})$ and the resistivity ρ as a function of an externally driven normalized current density $\check{J} = J/J_c$. Therefore, resistivity measurements in high-T_c superconductors can also be described by the EDM.

3.3.2. A simple shunted model for the resistivity below and above T_c. In high-T_c superconductors, direct measurements of I–V curves are limited to higher temperatures, where the EDM is not sufficient and additional effects have to be included.

In order to describe heuristically the resistivity $\rho(T, H, J)$ at low magnetic fields H, different behaviours will be attributed to separate fractions of the sample. These fractions are considered to be shunted in parallel, thus their conductivities σ are added: $\sigma = \sigma_N + \sigma_M + \sigma_A$. In the linear approximation the normal conductivity σ_N is $A/(T + C)$. The EDM is approximated by the power law $\sigma_M = A_M(T)(J/J_c)^{-1/b}$.

An Arrhenius form $\sigma_A = A_A \exp(U/T)$ describes the exponential regime below T_c. In addition, the excess conductivity in the paraconductive regime above T_c could be well described by the same Arrhenius form.

3.3.3. Arrhenius form for the excess conductivity above T_c. This heuristic Arrhenius form $\sigma_A = A_A \exp(U/T)$ has been checked with data of the excess conductivity $\sigma' = \sigma - \sigma_N$ from Soret and co-workers [20] measured above T_c in a single crystal of YBCO. Indeed, an Arrhenius form with $U \approx 1200$ K would also include, in their figure 2, the points outside the straight line that represents the Lawrence–Doniach (LD) form. Moreover, the resistance data of Friedmann and co-workers [21] measured in a single crystal of YBCO are 'very nearly linear' from 150–240 K, fitted with $\rho = aT + b$. Although they write 'the extreme linearity of ρ in this region (...) provides us with a basis for carefully studying the non-linear region below 150 K', the Aslamazov–Larkin (AL) and LD models fit well their data but with rather different values for a and b. When the values for a and b found between 150–240 K are used, only a small portion of the data agrees (see their figure 6). However, these data for σ' fit well σ_A between 96–150 K with $U = (1100 \pm 50)$ K, whereas below 96 K the data deviate, anticipating $T_c = 93$ K.

According to scaling near a second-order phase transition, the excess conductivity $\sigma' = \sigma - \sigma_N$ should follow a power law $\sigma' \propto \epsilon^{-p}$, where $\epsilon = (T - T_c)/T_c$, for the paraconductive region above T_c.

When interpreting the Arrhenius behaviour $\sigma_A \propto \exp(U/T) = c\,\epsilon^{p(\epsilon)}$ by a power law $\propto \epsilon^{p(\epsilon)}$, an ϵ-dependent exponent $p(\epsilon) = (1/\ln \epsilon^{-1})\{U/[T_c(1+\epsilon)] + \ln c\}$ would result. Thus a *continuously* changing exponent $p(\epsilon)$ for varying ϵ could indicate an Arrhenius behaviour.

Indeed, such a continuously changing slope is seen in the $\ln\sigma'$–$\ln\epsilon$ plot of figure 2 of [22] outside $-4 < \ln\epsilon < -2$, measured in a Bi–Sr–Ca–Cu–O pellet†.

3.3.4. The resistance of multilayered superconductors. At this point it might be interesting to note that (7), without percolating superconductivity, could be used to describe the resistance of multilayers prepared and investigated by Fischer and co-workers [23] at different fields H below and above T_c.

These thin films consist of superconducting layers separated by non-superconducting layers. The non-conducting layers seem to prevent a percolating supercurrent at low H, resulting in a wide range of Arrhenius behaviour $\rho \propto \exp(-U/T)$ below $\rho/\rho_N \approx 0.1$. However, the excess conductivity in the paraconductive region *above* T_c also seems to follow an Arrhenius behaviour, with a value for U comparable to the value found at low T. Therefore, the full measured temperature range could be approximated with a single nearly temperature independent value for U, if the description as a sum $\sigma = \sigma_N + \sigma'$ of normal σ_N and excess conductivity σ', which is well established to interpret the paraconductive region, is also applied below T_c, with $\sigma' \propto \exp(U/T)$ which describes well $\rho \propto \exp(-U/T)$ when $\sigma' \gg \sigma_N$. There might be a fortuitous correspondence of this Arrhenius behaviour with high-temperature excitations as evaluated for 2D Heisenberg models and observed in quasi-2D Heisenberg antiferromagnets [24].

3.3.5. Description of the resistivity of a granular YBCO sample. The simple shunted model for the resistivity will be applied to the resistance data in a YBCO sample measured by Wenk [25]. In order to simplify the fitting above T_c, the EDM prefactor $A_M(T) = a_M\sigma_N$ is chosen be proportional to σ_N. For $b = T/\tilde{E}$ the same temperature dependence $b \approx b_0\Theta(1-\Theta^2)^{n/2-2}(1+\Theta^2)^{-n/2}$ is used as in section 3.2.1. Furthermore, the critical current $J_c(T)$ is approximated by $J_c(T) \approx J_0(0)(1-\Theta^4)$. Since the EDM term is related to

† The data in figure 2 of [22] fitted with an Arrhenius $\sigma' \propto \exp(-\epsilon U/T)$ would yield, for the data at higher T, a value of about 2000 K for U, whereas the five data points at the lowest T would correspond to about 5000 K.

the temperature T_p, where the superconductivity percolates through the sample, the reduced temperature Θ is defined by $\Theta = T/T_p$ rather than T/T_c. For measurements performed at the same experimental current density J_{ex}, the ratio $D = J_{ex}/J_0$ is constant and the normalized current density $\check{J}(T) = D/(1-\Theta^4)$. However, for this form to result in $\check{J}(T) > 1$, $\check{J}$ is set to equal one, as for $T > T_p$.

The following forms have been used to fit the temperature dependence of the resistance R of a granular $YBa_2Cu_3O_{6.96}$ sample from the group of Kaldis† measured by Wenk [25]. First the parameters $A, C, U, F' = FA$ are fitted for $T > T_c$, with F' for an arbitrary chosen fixed $T_c = W$ in the Arrhenius term

$$\frac{1}{R} = \frac{1}{A}\left[\frac{1}{T+C} + F' \exp\left(\frac{U}{T} - \frac{U}{W}\right)\right]. \tag{7}$$

The additional parameters T_p, A_M, b_0, n, D are determined by fitting the full temperature range to the form

$$\frac{1}{R} = \frac{1}{A}\left[\frac{1 + A_M B_M}{(T+C)(1+A_M)} + F' \exp\left(\frac{U}{T} - \frac{U}{W}\right)\right] \tag{8}$$

with $B_M = \check{J}^{-1/b}$ when $\check{J} = D/(1-\Theta^4) < 1$ for $T < T_p$; otherwise $B_M = 1$. The resulting fit displayed in figure 9 has deviations $(R_{ex} - R_{model})/R_{ex}(103\,\mathrm{K})$ of the order of 10^{-3} above T_p and 10^{-2} below.

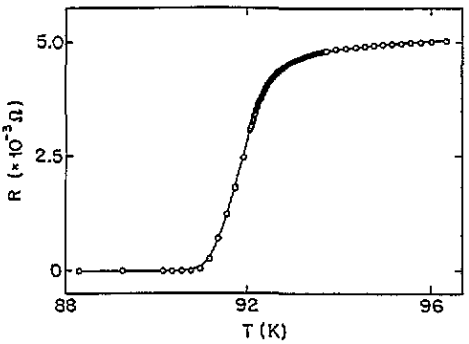

Figure 9. Points: resistance $R(T)$ of a granular $YBa_2Cu_3O_{6.93}$ sample (from Kaldis) measured by Wenk [25]. Curve: fit with (10) yielding $A = (1.49 \pm 0.08) \times 10^{-7}$, $C = (-28 \pm 3)$ K, $D = 4 \times 10^{-7}$, $b_0 = (3.9 \pm 0.1) \times 10^{-3}$, $F' = 0.10 \pm 0.02$, $U = (1.9 \pm 0.6) \times 10^4$ K, $T_p = (92.69 \pm 0.03)$ K, $n = 0.11$, for a chosen $W = 91$ K.

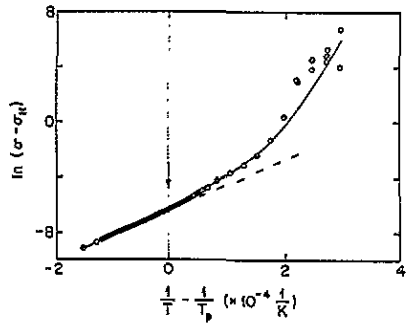

Figure 10. Points: logarithm of the excess conductivity $\ln(\sigma - \sigma_N)$ against $1/T - 1/T_p$ of a granular $YBa_2Cu_3O_{6.93}$ sample (from Kaldis) measured by Wenk [25]; curve: fit with (9); the broken line indicates the Arrhenius behaviour above T_p, the arrow marks T_p.

The Arrhenius behaviour in the paraconductive region and the onset of the percolating supercurrent at T_p is shown by plotting $\ln(\sigma - \sigma_N)$ against $1/T - 1/T_p$ in figure 10. The deviation from a straight line signals the onset of σ_M close to $T_p = 92.69$ K. Note the excellent fit in the paraconductive region and the clear deviation starting at T_p. Hence this

† E Kaldis of Eidgenössische Technische Hochschule Zürich, produced granular YBCO samples with a well defined oxygen content.

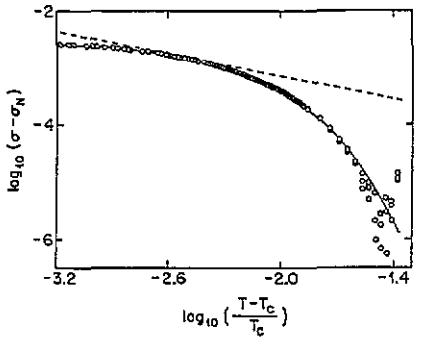

Figure 11. Log–log plot of the excess conductivity $\sigma - \sigma_N$ against the normalized temperature deviation $(T - T_c)/T_c$ with $T_c = 92.44\,K$ of Schneider and Keller [26]. Points: measured by Wenk [25] in a granular $YBa_2Cu_3O_{6.93}$ sample (from Kaldis). Full curve: fit with (9). Broken curve: exponent $p = 0.67$ of $\sigma - \sigma_N \propto (T - T_c)^p$ of [26].

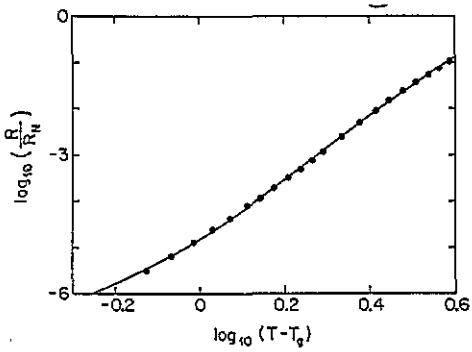

Figure 12. Log–log plot of the resistance ratio R/R_N against the temperature deviation $T - T_g$ with T_g of Gammel and co-workers [28]. Points: measured by Gammel and co-workers [28] in a YBCO probe at $H = 6\,T$. Curve: fit with (9) yielding $F' = 0.012 \pm 0.002$, $b_0 = 0.0213 \pm 0.0008$, $U = (11000 \pm 600)\,K$, $T_p = (78.95 \pm 0.07)\,K$.

type of plot is an alternative method to determine the temperature T_p as a substitute for T_c. In contrast, $\log(\sigma - \sigma_N)$ is plotted in figure 11 only above T_c against $\log(T/T_c - 1)$ for $T_c = 92.44\,K$ of Schneider and Keller [26]. The broken curve corresponds to their interpretation by a power law $\sigma' = \sigma - \sigma_N \propto (T - T_c)^{-p}$ with an exponent $p = 0.67$, the full curve is the Arrhenius excitation $\sigma' \propto \exp(U/T)$ where $U = 1.9 \times 10^4\,K$.

3.3.6. The resistivity at high fields H: transition to the glass state. The resistivity of high-T_c superconductors at high fields H is a more complex function of temperature T, since below T_c there is a gradual drop of the resistivity to a 'knee' observable at T_k for $\rho/\rho_N \approx 0.2 \div 0.3$, depending upon material and sample quality.

Below T_k, there is a region of thermal activation $R \propto \exp(-U/T)$ of Arrhenius type [27]. At lower temperatures, I–V curves are non-linear, resulting in a J-dependent resistivity.

The resistance R derived from isothermal I–V curves of a YBaCuO sample measured in the pV region by Gammel and co-workers [28] have been presented as 'significant evidence for a finite-temperature phase transition in the vortex state'. Here, the same data will be alternatively interpreted by the EDM combined with an Arrhenius excitation. Since Gammel and co-workers plotted the ratio R/R_N, where R_N is the linear extrapolation of the normal-state resistance, the following form for the normalized conductivity $\sigma/\sigma_N = R_N/R$ is found using (8) with $A_M \gg 1$, $C = 0$, $W = T_p$, and $n = 0$ in (4):

$$\frac{\sigma}{\sigma_N} = \left(\frac{D}{(1-\Theta^4)}\right)^{-(1-\Theta^2)^2/b_0\Theta} + TF'\exp\left[U\left(\frac{1}{T} - \frac{1}{T_p}\right)\right] \tag{9}$$

where $\Theta = T/T_p$. Hence the crude form $b = b_0\Theta(1 - \Theta^2)^{-2}$ is already sufficient. Furthermore, the ratio $D = J_{ex}/J_c(T = 0)$ was set equal to 10^{-10}. Only the parameters b_0, F', U, T_p were fitted. Moreover, the Arrhenius term described by F', U was relevant only for the data at the highest temperatures. Note that no T_g or T^* is involved, only $T_p \approx T_c$, representing in the model the temperature for the onset of percolating supercurrent at $H = 6\,T$. Figure 12 displays the EDM fit (line) and their data (points) in a log–log plot,

which yields a straight line for their interpretation by the power law $R/R_N \propto (T - T_g)^p$, assuming zero resistance at T_g and for their finite current density.

The EDM accounts only qualitatively for the deviation from linearity of the I–V data (points) at decreasing temperature (see figure 13(a) (curve).

In order to show the different extrapolations to lower temperatures, the data $\log(R/R_N)$ of Gammel and co-workers [28] are plotted in figure 13(b) against T, together with the lines for the models, with $R \to 0$ at $T_g = 74.0$K (broken curve) for the power law $(T - T_g)^{\nu(z-1)}$, and R/R_N falling below an obviously non-measurable value 10^{-15} around $T = 72$ K for the EDM (full curve).

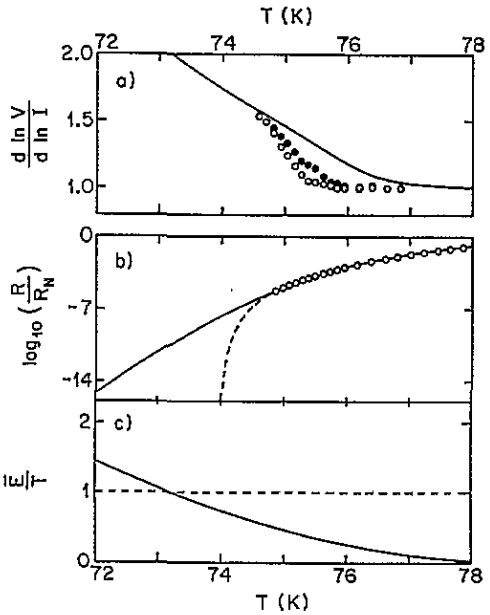

Figure 13. Points: measurements of Gammel and co-workers [28] in a YBCO probe at $H = 6$ T. Full curves: using (9) and fitting values of figure 12. (a) Deviation from linearity $\mathrm{d}\ln V/\mathrm{d}\ln I$ against temperature T. (b) $\log(R/R_N)$ against T with extrapolations of the fits to lower temperature. The fit of Gammel and co-workers [28] $R/R_N \propto (T - T_g)^{\nu(z-1)}$ (broken curve) extrapolates to zero resistance at $T_g = 74$ K, whereas the interpretation by the EDM (full curve) implies a drop to a finite but very low resistance. (c) The extrapolated value $1/b = \bar{E}/T$ against T using $b = b_0\Theta(1 - \Theta^2)^2$ and the fitting values of figure 12. Note that the EDM also implies a transition from 'fluid' to 'glassy' behaviour with a crossover temperature $T_{cro} \approx 73.2$ K where $\bar{E}/T = 1$.

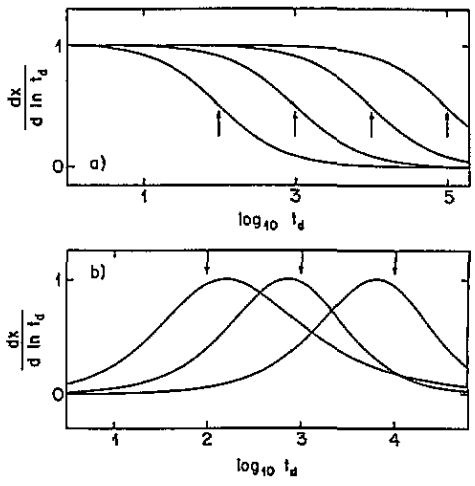

Figure 14. 'Memory' effect without a second step when derivatives $-\mathrm{d}x/\mathrm{d}(\ln t_d)$ of non-exponential functions $x(t)$ are plotted as a function of the *logarithm* of a *delayed* time t_d for $t = t_d + t_w$. (a) Derivative $-\mathrm{d}x/\mathrm{d}(\ln t_d)$ of a logarithmic decay $x(t) = 1 - \ln t$ against $\log t_d$ for $t_w = 10^q$ with $q = 2, 3, 4, 5$ (arrows). Note the inflection points at $t_d = t_w$. (b) Derivative $-\mathrm{d}x/\mathrm{d}(\ln t_d)$ of the power law $x(t) = t^{-b}$ against $\log t_d$ for $t_w = 100$, 1000, 10 000 (arrows) and $b = 0.6$, 1.3, 1.5, respectively. Note the extrema at $t_d = t_w/b$.

Although both interpretations fit well the measured data, the extrapolations to lower temperatures seem to be very different, but only in the region where no direct measurements are possible. However, the main point is that the scaling theory (ST) [29] and the EDM predict a sharp transition at T_g *only for the limit of vanishing current density* $J \to 0$ (see section 3.1.2 of [1]). For finite $J > 0$, both models also account for very small, but in principle finite,

(non-linear) resistivity below T_g. The discrepancy in figure 13(b) is due to the fact that the ST uses the prediction for $J \to 0$, whereas the EDM is applied for a very small but finite current density J. The fitting values for b_0 and T_p allow a crude extrapolation of $1/b = \bar{E}/T$ to lower temperatures, as shown in figure 13(c). The extrapolated temperature $T_{b=1} \approx 73.2\,\mathrm{K}$, where $\bar{E}/T = 1$, is not far from $T_g = 74\,\mathrm{K}$.

Since for $T_{b=1}$ the resistivity is $\rho \propto J$ in the EDM, this temperature corresponds to an I–V curve with $V \propto I^2$. This temperature could be determined from the I–V curves of Koch and co-workers [30] at higher V values. These curves exhibit a continuous increase of the slope s of $V \propto J^s$ in their $\log V$–$\log J$ curves. As displayed for the magnetic field of 4 T in their figure 1(b), $T_{b=1}$ is only slightly above their T_g since the broken line has, according to our interpretation, a slope $s = \partial \log V/\partial \log I = 2.4 \pm 0.1$, which deviates from their value 2.9 ± 0.2 in the text†.

In principle, $T_{b=1}$ could also be determined by decay measurements providing that the fast decay in the 'fluid' regime is observable. Using a variation of field scanning speeds and the high sensitivity of microwave absorption, interpreted with an adequately transformed EDM to account for the steady states, the ratio $T_{b=1}/T_c \approx 0.97$ at 0.5 T was found by interpolating the $b(T)$ values determined for a granular YBCO probe [3, 31].

3.4. Approximating the 'ageing' or 'memory' effect

3.4.1. Introductory remarks. The 'ageing' or 'memory' effect is considered to be a strong evidence for a spin glass [10, 32]. When a sample is, for example, field cooled at time t_A, and when later at time t_B the field is set to zero, the decaying non-equilibrium magnetization M might exhibit a special feature at time t_C around $t_B + (t_B - t_A)$ when plotted as a function of the logarithm of a 'delayed' time t_d starting at time t_B. Similar effects are seen after zero field cooling at t_A and a field step at t_B. Since the appearance of the feature seems to remember the length of the 'waiting time' $t_w = t_B - t_A$, it is also called a 'memory' effect occurring around $t_d \approx t_w$.

Theoretically, this effect is attributed to a distribution that changes already during the waiting time with, for example, parallel or hierarchical relaxation, as described by Fisher and Huse [10] or Sibani and Hoffmann [33], respectively. Lundgren and co-workers [34] evaluated from measured decay curves the distributions of the relaxation times, which shift to larger relaxation times for increasing waiting times.

Rossel and co-workers [15] described qualitatively the memory effect by superimposing two distributions, D_A and D_B, of activation energies. The first, D_A, starts to decay at the time t_A of quenching the temperature; the second, D_B, starts at time t_B of a field step. Hence the first distribution is already 'ageing' during the waiting time t_w, while the second distribution starts to decay at t_B. The important point is that both distributions start with a large fraction exhibiting short relaxation times. The superimposed distribution might show a change of the macroscopic decay around the time $t \approx t_w$, with the delayed time $t = 0$ starting at t_B, as observed in spin glasses [35] and in high-T_c superconductors [15], for example.

Before these measurements are described by a superposition of decay functions of the EDM, an interesting feature inherent in non-exponential decay functions will be discussed.

† This implies that the scaling relation $s = (z + 1)/2$ for 3D would yield $z = 3.8$, instead of their $z = 4.8 \pm 0.2$. This discrepancy should be clarified, since they wrote 'for $d = 3$ we expect $z > 4$ as in the Ising spin glass' ···'gives $z = 4.8 \pm 0.2$ in good agreement with our expectations for a vortex–glass transition in 3D' ··· 'we find a value of $z \simeq 4.8$, in excellent agreement with the estimate of z obtained independently from the I–V curve at T_g.' Moreover, it is rather surprising that this discrepancy between figure and text is repeated in the review article [29].

3.4.2. A 'memory' feature present without a second step. As described above, a 'memory' feature appears after a double-step procedure remembering the time interval t_w between these steps. It is an intriguing fact that a 'memory' feature is already present after a single-step procedure at t_A, if (i) the decay is strongly non-exponential, and (ii) the decay is plotted as the *logarithm* of a *delayed* time t_d starting at an arbitrary chosen time t_B, thus after a fictive waiting time t_w.

In particular, a straightforward calculation reveals that a *logarithmic* decay $x(t) \propto 1 - b \ln t$ with $t = t_d + t_w$ exhibits an *inflection point* at $t_d = t_w$ for arbitrary t_w in its derivative $-dx/d(\ln t_d) \propto d \ln(t_d + t_w)/d(\ln t_d)$ with respect to the logarithm of the delayed time $t_d = t - t_w$ (see arrows in figure 14 (top)).

Thus, an 'ageing' or 'memory' *inflection point* 'appears' in the derivative of decay data around $t_d \approx t_w$ without a second step at the time t_B, if the decay form is close to $1 - b \ln t$, as discussed in the next section for a superconductor (see figure 15).

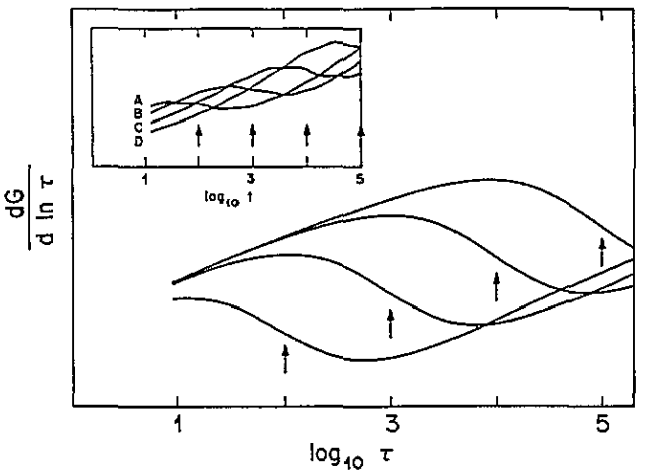

Figure 15. Approximating the memory effect: derivative $dG/d(\ln \tau)$ against $\log \tau$ of $G(b, \tau) = (1 - a)g(b, \tau + \tau_w) + ag(b, \tau)$, see (10), with $a = 0.7$, $b = 0.05$, $\tau_0 = 1$, and waiting times $\log_{10} \tau_w = 2, 3, 4, 5$. The arrows mark $\tau = \tau_w$. Inset: similar data evaluated by Sibani and Hoffmann [33] with their hierarchical model from their figure 3. Note that both methods result in a jump around $\tau = \tau_w$.

Moreover, a decay $x(t)$ in the form of a *power law* t^{-b} will exhibit an *extremum* of the derivative $-dx/d(\ln t_d) = -d(t_d + t_w)^{-b})/d(\ln t_d)$ at $t_d = t_w/b$ when plotted as a function of the logarithm $\ln t_d$ of the delayed time t_d (see arrows in figure 14 (bottom)) with $b = 0.6$, 1.3 and 1.5 for $t_w = 100$, 1000 and 10 000, respectively.

Thus an 'ageing' or 'memory' *extremum* 'appears' close to $t_d \approx t_w$ in the derivative for decay functions close to a power law t^{-b} when $b \approx 1$, similar to measurements in metallic spin glasses displayed as a function of the *logarithm* of a *delayed* time in the next section (figure 16).

3.4.3. Approximating the 'memory' effect with the EDM. Following the proposal of Rossel [15], the memory effect is approximated with the EDM by the superposition of $g_1(b_1, \tau_d + \tau_w)$ and $a\, g_2(b_2, \tau_d)$ with the prefactor a characterizing the sign and the magnitude of the second step, yielding the non-normalized observable $G_{\text{ageing}}(\tau_d)$:

$$G_{\text{ageing}}(b_1, b_2, a, \tau_w; \tau_d) = g_1(b_1, \tau_d + \tau_w) + a\, g_2(b_2, \tau_d). \tag{10}$$

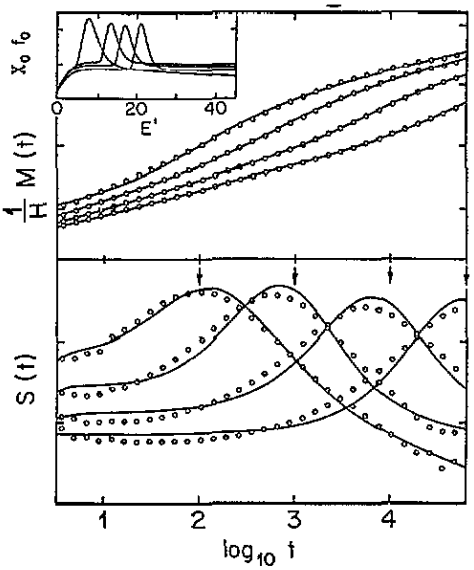

Figure 16. 'Ageing' effect in the amorphous metallic spin glass $(Fe_xNi_{1-x})_{75}B_{16}P_6Al_3$ of Svedlindh and co-workers [36]. Points: zero field cooled susceptibility $[(1/H)M(t)]$ and corresponding relaxation rate $[S(t) = (1/H)dM/d\ln t]$ at different waiting times (t_w = 10^2, 10^3, 10^4, and 10^5 s) plotted against $\log_{10} t$ where $t = t_d$ starts at the field step to $H = 0.1$ G. Curves: fits with (11) of the EDM with the above t_w, and $b_1 = 0.6$, 1.3, 1.5, 2.7; $b_2 = 0.02$, 0.02, 0.01, 0.01; $r_{0,1,2} = 0.7$, 0.7, 0.9, 1.4; $t_{in,1} = 4$, 8, 3, 5 s; $t_{in,2} = 1.5$, 1.5, 0.8, 2.1 s; $c = 0.976$, 0.977, 0.949, 0.932; $X_0 = 1.1$, 1.0, 0.4, 0.3; respectively. Inset: distribution functions $X_0 f_0(E')|_{t_d=0}$ of activation energies $E' = E/T$ evaluated with the above EDM parameters.

Assuming first $b_1 = b_2 = b$ and $b \ll 1$, resulting in a decay which is close to logarithmic $\approx 1 - b\ln\tau$ for $\tau_w/b \gg 1$, it is instructive to write the derivative $-(1/b)dG/d\tau_d$ with respect to the delayed time τ_d:

$$-\frac{1}{b}\frac{dG}{d\tau_d} \approx \frac{1}{\tau_d + \tau_w} + \frac{a}{\tau_d}. \tag{11}$$

If $|a| \approx 1$, the slope is around a/τ_d and $(a+1)/\tau_d$ for times $\tau_d \ll \tau_w$ and $\tau_d \gg \tau_w$, respectively, indicating logarithmic decays of $G(\tau_d)$ for both regimes. A changeover between these regimes occurs around $\tau_d \approx \tau_w$, thus 'memorizing' the initial waiting time t_w.

This effect is shown in figure 15 by displaying the derivative $dG/d(\ln\tau_d)$ for different waiting times τ_w, to be compared with the numerical result of the hierarchical model of Sibani and Hoffmann [33] (their figure 3 is displayed as the inset in figure 15). Note that in both cases $\tau_d = \tau_w$ corresponds to the turning point, as evaluated in section 3.4.2 for a logarithmic decay after a single step. Thus this 'memory' effect is already present when g_1 is plotted as a function of $\ln\tau_d$.

Probably the clearest experimental evidence of the 'ageing' effect has been found in dilute metal spin glasses, with the measurements of Svedlindh and co-workers [36] in the amorphous metallic system $(Fe_xNi_{1-x})_{75}B_{16}P_6Al_3$ as an example (see the points in figure 16). The curves represent a fit with a normalized superposition of the two-parameter EDM functions

$$g_{ageing}(\tau_d) = (1-c)g_1^{(2)}(b_1, \tau_{in,1}; \tau_d + \tau_w) + cg_2^{(2)}(b_2, \tau_{in,2}; \tau_d) \tag{12}$$

where $\tau_i = r_{0,i} t_i$.

Although the fit is not perfect for the derivative, the curves clearly show all the measured features. The evaluated initial times t_{in} are of the order of one second, thus of the order of the time for the cooling procedure.

The EDM could be interpreted as an independently decaying distribution of activation energies $E' = E/T$. Such distributions for $t_d = 0$ are plotted in the inset in figure 15, evaluated with the fitting parameters of the EDM. The main feature is a pronounced peak at an energy that increases due to the 'ageing' after the first step, very similar to the distributions of relaxation times displayed by Lundgren and co-workers [34] as evaluated from decay measurements in the metallic spin glass Cu–4at.%Mn. The second step creates only a rather flat additional distribution, which does not contribute to the 'ageing' feature.

On the other hand, interpreting the EDM as being due to a single effective energy $U_{eff}(x)$ increasing as a function of the decaying observable x, thus assuming a process which is homogeneous, would result in the same 'ageing' features. Therefore, the 'ageing' feature is, in our opinion, a consequence of specific non-exponential decay forms rather than a unique indication for a spin glass behaviour.

4. Concluding summary

The 'elementary decay model' (EDM) introduced in [1] has been applied here to various data measured in superconductors and in a metallic spin glass.

The effective activation energy U_{eff} in a high-T_c superconductor obtained from measurements of van der Beek and co-workers [5] using a method proposed by Maley and co-workers [4] is well described by the EDM. These data and the EDM are both close to $U_{eff} \propto \ln(1/\check{J})$, where $\check{J} = J/J_c$ is the normalized current density. Thus the EDM agrees well with the microscopically exact solution $U_{eff} \propto \ln(1/\check{J})$ for the vortex motion controlled by intrinsic pinning in a layered system found by Blatter and co-workers [37] and used by Vinokur and co-workers [38], whereas the power law $U_{eff} \propto (\check{J})^{-\mu}$ widely used for collective creep [6, 7, 9] results in a continuously changing exponent μ.

Since decay and I–V curves have the same origin, a combination of such measurements in $YBa_2Cu_3O_x$ (YBCO) was used by Sandvold and Rossel [11] and interpreted with the collective creep theory. The same theory was used to fit decay measurements of Svedlindh and co-workers [12] in an extreme type-II superconductor. Both papers were analysed as to what extent other models can be excluded, especially the model of Blatter and co-workers [37] with $U_{eff} \propto -(1/b)\ln\check{J}$ implying $x(t) \propto t^{-b}$, which is very close to the EDM.

The decay in a heavy fermion superconductor, reported by Pollini and co-workers [13], an example of a stretched exponential decay known as the Kohlrausch function $\exp[-(r_0 t)^{\beta}]$, could not be described by the closed form of the EDM. However, keeping the idea of the EDM of an initial distribution which decays independently, a distribution was found which is close to a Gaussian at an intermediate time.

Since the temperature dependence of the decay is not part of the EDM, established forms for the temperature dependence of the pinning energy were used for testing the temperature dependence in high-T_c superconductors. The logarithmic rate $-\mathrm{d}X/\mathrm{d}(\ln t)|_{t_0}$ and the normalized logarithmic rate $-\mathrm{d}\ln X/\mathrm{d}(\ln t)|_{t_0}$ at a fixed time t_0 of various measured data [14, 18] were compared with the corresponding values evaluated with the EDM using a temperature-dependent mean activation energy $\tilde{E}(T)$ for $b = T/\tilde{E}$.

Hagen and Griessen [14] evaluated a distribution of pinning energies from decay data measured at intermediate times using a superposition of logarithmic decay forms and

assuming an appropriate temperature dependence. Their distribution coincides with the distribution of the EDM at intermediate decay times.

Since decay is connected to electric resistivity, the EDM is also applied to interpret I–V curves measured in high-T_c superconductors. In order to interpret the fluctuations around and above T_c, an additional term of Arrhenius type $\propto \exp(-E/T)$, corresponding to high-temperature excitations in a 2D Heisenberg model [24], was introduced, which fits well the whole regime above T_c in a YBCO granular sample [25] and the whole temperature range in multilayered YBCO films as reported in [23]. This term combined with the EDM fits well the resistivity of a granular YBCO sample and serves as a determination of a temperature T_p for the onset of percolating supercurrent. Moreover, the pV measurements of Gammel and co-workers [28] were analysed. Deviations from the scaling theory (ST) [29] only occur in the region of non-measurable small resistivity because Gammel and co-workers [28] fitted the data with the prediction of the ST for the limit of vanishing current density $J \to 0$, whereas the EDM is applied for small but finite J, for which the ST also does not predict a sharp transition.

It is a very open question why the EDM using the elementary assumption of 'the existence of energy barriers of arbitrary heights' which Nattermann [9] considered to be the 'most important ingredient' of his 'scaling approach to pinning', combined with an established temperature dependence for the mean pinning energy $\bar{E}(T)$, is already sufficient to account certainly not for all, but for many, experimental data of high-T_c superconductors, which confirm the scaling theory.

The 'ageing' or 'memory' effect measured in spin glasses and superconductors was interpreted by the EDM, in particular the measurements of Svedlindh and co-workers [36]. A rather surprising result is that a 'memory' feature would also appear without the application of a second step after a waiting time, since this feature is a result of plotting a non-exponential decay as a function of the logarithm of a delayed time and is, therefore, not directly related to spin glass behaviour.

Finally, this work shows again that investigations of only one macroscopic observable are not sufficient to discriminate between *uniform* and *distributed* features, an old problem of solid state physics. Additional investigations, such as a determination of the distribution of *local* magnetic fields as measured by myon spin rotation, performed by Harshman and co-workers [39], and a determination of the distribution of pinning energies using the temperature and frequency dependence of the noise, performed by Ferrari and co-workers [16], would be welcome.

Acknowledgments

The authors would like to thank G Blatter, E H Brandt, T H Geballe, P Granberg, C W Hagen, H Keller, P H Kes, A P Malozemoff, A C Mota, K A Müller, T Nattermann, A Pollini, C Rossel, T Schneider and M Warden for helpful comments, and P Wenk and D Zech for their resistivity data. This work has been supported by the Swiss National Science Foundation.

References

[1] Erhart P, Portis A M, Senning B and Waldner F 1994 *J. Phys.: Condens. Matter* **6** 2893
[2] Müller K M, Takashige M and Bednorz J G 1987 *Phys. Rev. Lett.* **58** 1143

[3] Erhart P, Senning B, Mini S, Fransioli L, Waldner F, Drumheller J E, Portis A M, Kaldis E and Rusiecki S 1991 *Physica* **185–9C** 2233
[4] Maley M P, Willis J O, Lessure H and McHenry M E 1990 *Phys. Rev.* B **42** 2639
[5] van der Beek C J, Kes P H, Maley M P, Menken M J V and Menovsky A A 1991 *Physica* **185–9C** 2507
[6] Feigel'man V M, Geshkenbein V B Larkin A I and Vinokur V M 1989 *Phys. Rev. Lett.* **63** 2303
[7] Fisher D S, Fisher M P A and Huse D A 1991 *Phys. Rev.* B **43** 130
[8] Vinokur V M, Kes P H, and Koshelev A E 1990 *Physica* **168C** 29
[9] Nattermann T 1990 *Phys. Rev. Lett.* **64** 2454
[10] Fisher D S, Huse D A 1988 *Phys. Rev.* B **38** 373
[11] Sandvold E and Rossel C 1992 *Physica* **190C** 309
[12] Svedlindh P, Niskanen K, Norling P, Nordblad P, Lundgren L, Rossel C, Sergent M, Chevrel R and Potel M 1991 *Phys. Rev.* B **43** 2735
[13] Pollini A, Mota A C, Visani P, Juri G, Teruzzi T and Franse J J M 1991 *Physica* **185–9C** 2625
[14] Hagen C W and Griessen R 1989 *Phys. Rev. Lett.* **62** 2857
[15] Rossel C, Maeno Y and Morgenstern I 1989 *Phys. Rev. Lett.* **62** 681
Rossel C 1990 *Relaxation in Complex Systems and Related topics (NATO ASI B Phys.* **222**) ed I A Campbell and C Giovannella (New York: Plenum) pp 105–12
[16] Ferrari M J, Johnson M, Wellstood F C, Clarke J, Mitzi D, Rosenthal P A, Eom C B, Geballe T H, Kapitulnik A and Beasley M R 1990 *Phys. Rev. Lett.* **64** 72
[17] Malozemoff A P and Fisher M P A 1990 *Phys. Rev.* B **42** 6784
[18] Griessen R, Lensink J G and Schnack H G 1991 *Physica* **185–9C** 337
[19] Theuss H 1993 *Physica* **208C** 155
[20] Soret J C, Ammor L, Martinie E, Lecomte J, Odier P, and Bok J 1993 *Europhys. Lett.* **21** 617
[21] Friedmann T A, Rice J P, Giapintzakis John, and Ginsberg D M 1989 *Phys. Rev.* B **39** 4258
[22] Balestrino G, Nigro A, Vaglio R and Marinelli M 1989 *Phys. Rev.* B **39** 12264
[23] Triscone J-M, Antognazza L, Brunner O, Miéville L, Karkut M G, van der Linden P, Perenboom J A A J and Fischer Ø 1991 *Physica* **185–9C** 210
Antognazza L, Brunner O, Miéville L, van der Linden P, Perenboom J A A J, Triscone J-M, and Fischer Ø 1991 *Physica* **185–9C** 2079
Brunner O, Karkut M G, Antognazza L, Triscone J-M, and Fischer Ø 1991 *Physica* **185–9C** 2081
[24] Waldner F 1992 *J. Magn. Magn. Mater.* **104–7** 793
[25] Wenk P 1993 Private communication
[26] Schneider T and Keller H 1993 *Physica* **207C** 366
[27] Palstra T T M, Batlogg B, Schneemeyer L F and Waszczak J V 1988 *Phys. Rev. Lett.* **61** 1662
[28] Gammel P L, Schneemeyer L F and Bishop D J 1991 *Phys. Rev. Lett.* **66** 953
[29] Huse D A, Fisher M P A and Fisher D S 1992 *Nature* **358** 553
[30] Koch R H, Foglietti V, Gallagher W J, Koren G, Gupta A, and Fisher M P A 1989 *Phys. Rev. Lett.* **63** 1511
[31] Erhart P, Drumheller J E, Portis A M, Senning B, Mini S, Fransioli L, Kaldis E, Rusiecki S and Waldner F 1992 *J. Magn. Magn. Mater.* **104–7** 487
[32] Morgenstern I 1990 *Earlier and Recent Aspects of Superconductivity* ed J GBednorz and K A Müller (Berlin: Springer) p 240
[33] Sibani P and Hoffmann K H 1989 *Phys. Rev. Lett.* **63** 2853
[34] Lundgren S, Svedlindh P, Nordlad P and Beckman O 1983 *Phys. Rev. Lett.* **51** 911
[35] Lundgren L 1988 *J. Physique* **49** C8 1001
[36] Svedlindh P, Granberg P, Nordblad P, Lundgren L and Chem H S 1987 *Phys. Rev.* B 35 268
[37] Blatter G, Ivlev B I and Rhyner 1990 *Eidgenössische Technische Hochschule Zürich'report*
[38] Vinokur V V, Feigel'man M V, Geshkenbein V B *Phys. Rev. Lett.* **67** 915
[39] Harshman D R, Fiory A T and Cava R J 1991 *Phys. Rev. Lett.* **66** 3313